Basin-Scale Water Resources Assessment in Oklahoma under Synthetic Climate Change Scenarios Using a Fully Distributed Hydrologic Model

Lorena Liuzzo, Ph.D.[1]; Leonardo V. Noto[2]; Enrique R. Vivoni[3]; and Goffredo La Loggia[4]

Abstract: Climate change resulting from the enhanced greenhouse effect is expected to have significant implications for the hydrological cycle. Several studies have pointed out the importance of basin-scale investigations for determining regional impacts on water resources, including the effects of floods and droughts. In this study, a fully distributed hydrologic model is used to assess the potential impacts of climate change on water availability in a basin in Oklahoma (United States). With this aim, the hydrologic model was applied for current conditions as well as under the hypotheses of climate variations represented by scenarios consistent with a climatic trend analysis generated using a stochastic weather model. Hydrologic simulations indicate that streamflow and evapotranspiration reflect variations in precipitation differently. Positive trends in precipitation result in an increase in surface and groundwater resources, while evapotranspiration is only affected slightly due to the higher soil moisture in the basin. Sensitivity analyses of the evapotranspiration and runoff changes to precipitation variations confirm these results. Comparisons of the impacts of the precipitation trend on surface and groundwater resources showed that the increase of surface water resources is ∼3 times greater, implying the groundwater system is affected less by climate change. The use of a distributed model also provided insight on the spatial variation of the water balance components. Results showed that the most significant increases of soil moisture (∼60%) are located along the river network and in the flat areas of the basin, characterized by a higher frequency of saturation excess runoff. In summary, climate change scenarios in this region produced an increase in water resources that can have beneficial impacts, but these positive effects are tempered by the increasing potential for flood risk. The increase of this risk has been evaluated as well in this analysis.

Introduction

Water resources development and management require an understanding of basic hydrologic processes and an investigation of the effects that factors such as climate and land use change can produce on water resource availability. The latest report of the Intergovernmental Panel on Climate Change (IPCC 2007) re-affirms that climate is changing in ways that cannot be accounted for by natural variability, since human activities have become a dominant force, and are responsible for most of the warming observed over the past 50 years. Climate change is likely to have significant impacts on the hydrologic cycle, affecting water resources systems throughout the globe (e.g., Leavesley 1994; Arnell 1999; Lettenmaier et al. 1999; Christensen et al. 2004).

Hydrologic models are important tools to investigate the relation between water resources and climate change. A large number of studies describe the application of hydrologic models to the assessment of the potential effects of climate change on surface and groundwater resources (Lettenmaier et al. 1999). In order to accurately describe hydrologic processes, under stationary and changing climate conditions at different spatial and temporal scales, the use of a distributed physically based model can be useful. A distributed modeling approach is suggested for modeling the dynamics of streamflow generation, since it allows one to include detailed information on topography, land use, soils and vegetation, and also to reproduce the spatial and temporal variability of the hydrologic processes (Ivanov et al. 2004a,b; Vivoni et al. 2007).

In previous studies, researchers typically make use of time series of observed precipitation and temperature, modified with information from climate simulations, in hydrologic models to gain insight on how the hydrologic cycle might change. A large number of these studies analyzed the impacts of climate change in large areas or at the basin scale in the United States (Nemec and Schaake 1982; Duell 1994; Wilby et al. 1999; Wolock and

[1]Dipartimento di Ingegneria Idraulica ed Applicazioni Ambientali, Università degli Studi di Palermo, Viale delle Scienze, 90128 Palermo, Italy (corresponding author). E-mail: liuzzo@idra.unipa.it

[2]Researcher, Dipartimento di Ingegneria Idraulica ed Applicazioni Ambientali, Università degli Studi di Palermo, Viale delle Scienze, 90128 Palermo, Italy. E-mail: valerio@idra.unipa.it

[3]Professor, School of Earth and Space Exploration and School of Sustainable Engineering and the Built Environment, Arizona State Univ., Tempe, Arizona 85287–1404. E-mail: vivoni@asu.edu

[4]Professor, Dipartimento di Ingegneria Idraulica ed Applicazioni Ambientali, Università degli Studi di Palermo, Viale delle Scienze, 90128 Palermo, Italy. E-mail: glal@idra.unipa.it

McCabe 1999; Wood et al. 2004). One of these studies, carried out by Nash and Gleick (1991, 1993), focused on the evaluation of the effects of climate change on seasonal and annual runoff in several subbasins of the Colorado River. In this analysis, the writers found that annual runoff, estimated using a conceptual model, was more sensitive to changes in precipitation than to changes in temperature.

Hamlet and Lettenmaier (1999) analyzed the implications of future climate predictions derived from four general circulation models (GCMs) to evaluate possible future changes to Pacific Northwest climate and the surface water response of the Columbia River. Quasi-stationary decadal mean temperature and precipitation changes were used to perturb historical records of precipitation and temperature to create inferred conditions for 2025, 2045, and 2095. In future climate scenarios, the projected increase in temperature leads to increases in the proportion of winter precipitation, falling as rain, and in the frequency of winter flooding, while a decrease in late spring and summer streamflows occurred. Lettenmaier et al. (1999) studied the impacts of climate change in six North American watersheds representing a variety of physiographic and geographic conditions. While the implications of climate change for these basins were different across the study regions, variations in runoff had more correlation to changes in precipitation than to changes in temperature.

With regard to forcing hydrologic models, most studies use GCMs in the assessment of the impacts of climate change. The current generation of GCMs are typically unable to deliver detailed results to describe climate variability at the regional scale (IPCC 1995), limiting their use for water resources impact studies (Grotch and MacCracken 1991). As a result, alternative means are needed to derive climate forcing for regional studies that ensure consistency among the meteorological variables in space and time (Werner and Gerstengarbe 1997). One feasible approach is the use of a stochastic weather generator (SWG) to estimate climate change at the basin scale based on historically observed data at a gauged site. As shown by Yates et al. (2003), SWGs can be used to simulate regional climate scenarios consistent with the global change predictions.

Weather generators generally have a similar structure, in which precipitation is considered the primary variable (Wilks and Wilby 1999). One of the most used stochastic weather models is the Richardson (1981) WGEN model of daily precipitation, maximum and minimum temperature, and solar radiation. Parlange and Katz (2000) extended the Richardson model to include additional variables, including daily mean wind speed and dew point. Recently, weather generators have been used in climate change studies to produce daily series of hydrometeorological variables for scenarios of future climate (Wilks 1992; Mearns et al. 1997; Semenov and Barrow 1997). While most SWGs use a daily time step, a few hourly scale models have been provided in more recent studies (Degelman 1991; Ivanov et al. 2007).

In this study, the hydrologic impacts of climate change have been investigated at the basin scale in the Southern Great Plains. This region has been selected since it has undergone relatively minor land use change, regulation and urbanization in the past 50 years. Moreover, the subhumid climate in the region leads to a basin response that is sensitive to precipitation variations (Garbrecht et al. 2001; McCarthy et al. 2001). In the study region, Garbrecht and Rossel (2002) identified an increase in precipitation over the last two decades of 20th century. In a following study, Garbrecht et al. (2004) assessed the hydrologic impacts of decade-scale variations in annual and seasonal precipitation by analyzing observations from ten watersheds in the Southern Great Plains, including the Baron Fork at Eldon, Okla. In this region, a positive trend in precipitation had a marked effect on streamflow and a comparatively weaker impact on evapotranspiration.

According to Garbrecht et al. (2004), in all the watersheds the mean annual precipitation increased by 12% on average during the period 1981–2001. In particular, Oklahoma experienced the greatest precipitation increase (about 19%). For the Baron Fork basin, the fall season captured about one-half of the annual increase, while winter captured another third, and spring the remainder. Summer remained substantially unchanged in the historical record. Hence, fall and winter together captured ~80% of the annual precipitation increase in the 20-year period. For the same region, IPCC (2007) indicates the existence of an increasing trend in precipitation ranging from 20 to 40% per century. With regard to temperature in the region, IPCC (2007) does not reveal a statistically significant trend. Due to the precipitation trend, Garbrecht et al. (2004) also detected a 64% increase in streamflow, but only a 5% increase in evapotranspiration, calculated as a water balance residual.

In order to investigate the effects of this positive precipitation trend on surface and groundwater resources, two test basins in the Southern Great Plains have been selected, the Baron Fork at Eldon and its subbasin Peacheater Creek at Christie (Oklahoma). The triangulated irregular network (TIN)-based real-time integrated basin simulator (tRIBS) model (Ivanov et al. 2004a; Vivoni et al. 2007), has been applied to the test basins under current climate conditions and in a series of synthetic climate scenarios generated with a SWG conditioned on future projections of the observed historical trends. The selection of the two test basins is due the fact that the model has been calibrated using streamflow observations at Baron Fork and Peacheater Creek (Ivanov et al. 2004b) in the Distributed Model Intercomparison Project, described in detail in Smith et al. (2004).

The hydrometeorological forcings required by the tRIBS model have been simulated using an hourly SWG (Ivanov et al. 2007) taking into account the trends detected during a climate trend analysis. A nonparametric test of precipitation and temperature highlighted the presence of a general increase of precipitation and absence of a statistically significant trend in temperature. Scenarios constructed with the SWG and conditioned on the trend analysis are not intended to explicitly represent real future climate. Instead, these serve as scenarios of potential climate alterations that can be used to estimate of the effect of climate change on hydrologic processes. The distributed modeling approach in this study has the advantage of providing a detailed understanding of the effects of climate trends on the hydrologic processes involved in surface and groundwater supply. Moreover, the use of a distributed model also allows identifying the sensitivity of water balance components and their spatial variation to climate trends. Furthermore, the application of a modeling approach can provide physical explanations to results obtained by Garbrecht et al. (2004), based on inferences from historical observations, since it allows one to calculate directly the components of the water and energy balance.

Methods

Detection of Trends in Hydrometeorological Data

The presence of trends in hydrometeorological data, associated with climate change, has received considerable attention. Several studies focused on the United States have detected that, in many

areas, annual precipitation is undergoing a slow increase (Karl et al. 1996; Karl and Knight 1998; Easterling et al. 2000). Hu et al. (1998) detected a gradual increase in precipitation since the mid-1960s in the central United States, while Kunkel et al. (1999) showed an upward trend at the rate of 3% per decade for the period 1931–1996, over the southwest United States and the Great Plains. With regard to the study region, Garbrecht and Rossel (2002) and Garbrecht et al. (2004) identified a 12% increase in mean annual precipitation over the period 1981–2001. To confirm these results, a trend analysis of precipitation and temperature was carried out here, with the aim to quantify the direction and magnitude of potential future climate variations.

Several statistical procedures have been used for detection of gradual trends, in particular parametric and nonparametric tests. In this study, the nonparametric Mann-Kendall test for trend detection (Mann 1945; Kendall 1962) has been used. This test identifies the presence of a trend, without making an assumption about the distribution properties. Moreover, nonparametric methods are less influenced by the presence of outliers. In a trend test, the null hypothesis H_0 is that there is no trend in the population from which the data are drawn; while hypothesis H_1 is that there is a trend in the records. The test statistic, Kendall's S, (Kendall 1962), is calculated as

$$S = \sum_{i=1}^{n-1} \sum_{j=i+1}^{n} \text{sign}(y_j - y_i) \qquad (1)$$

where $y=$ data values at times i and j and $n=$ length of the data set and

$$\text{sign}(\vartheta) = \begin{cases} 1 & \text{if } \vartheta > 0 \\ 0 & \text{if } \vartheta = 0 \\ -1 & \text{if } \vartheta < 0 \end{cases} \qquad (2)$$

Under the null hypothesis that y_i are independent and randomly ordered, the statistic S is approximately normally distributed when $n \geq 8$, with zero mean and variance as follows:

$$\sigma^2 = \frac{n(n-1)(2n+5)}{18} \qquad (3)$$

The standardized test statistic Z_S is computed by

$$Z_S = \begin{cases} \dfrac{S-1}{\sigma} & \text{if } S > 0 \\ 0 & \text{if } S = 0 \\ \dfrac{S+1}{\sigma} & \text{if } S < 0 \end{cases} \qquad (4)$$

and compared with a standard normal distribution at the required level of significance. If the significance level α is set equal to 0.05, the null hypothesis is verified when $|Z_s| \geq 1.96$. A positive value of Z_S indicates an increasing trend and vice versa. The magnitude of trends was evaluated using a nonparametric robust estimate determined by Hirsch et al. (1982)

$$\beta = \text{Median}\left(\frac{x_j - x_l}{j - l}\right) \quad \forall \, l < j \qquad (5)$$

where $x_l =$ lth observation.

In order to evaluate the presence of a regional trend in temperature, we used the Regional Average Kendall's S (S_m) computed as

$$S_m = \frac{1}{m} \sum_{i=1}^{m} S_k \qquad (6)$$

where $S_k=$ value of Kendall's S statistic in kth station in a region with m stations.

If stations are uncorrelated in space, the standardized test statistic can be calculated with (Douglas et al. 2000)

$$Z_m = \frac{S_m - E(S_m)}{\sigma/\sqrt{m}} \qquad (7)$$

where $E(S_m)=$ expected value of S_m and $\sigma=$ same as defined earlier. The significance of Z_m can be computed from the cumulative distribution function (CDF) of a standard normal variate.

Since the results of the Mann-Kendall test can be affected by the cross correlation between measurement stations (Lettenmaier et al. 1994), a bootstrap resampling approach (Efron 1979) has been used herein. In this way, it has been possible to determine the critical value for the percentage of stations expected to show a trend by chance. The null hypothesis for our trend tests was that the annual, monthly, seasonal data exhibit no trend, are spatially correlated and serially independent. We used the bootstrap method to evaluate the CDF of S_m, in order to determine the field significance associated with S_m computed from historical data.

Generation of Climate Scenarios

The SWG of Ivanov et al. (2007) was used to generate the hydrometeorological variables for each climate scenario. The weather generator allows simulation at a given geographic location of precipitation, total cloud cover, incoming shortwave radiation, air temperature, humidity, and wind speed. It can be used to produce long periods of synthetic weather records from a limited amount of input data. Furthermore, it has the capability of reproducing the diurnal cycle of hydrometeorological variables that are essential for hydrological simulations that consider the coupled water and energy balance in distributed locations within a watershed.

The SWG considers precipitation to be the key driver of the simulated hydrometeorological conditions, which leads to a consistent covariation of the other variables. Rainfall is simulated according to the following procedure: at some initial time t_0, an interstorm duration t_b is generated from an exponential distribution. The period $[t_0, t_0 + t_b]$ is considered dry. When the time reaches $[t_0 + t_b]$, the storm duration t_r is generated. Using the value set for t_r, a storm depth h is generated from a gamma distribution. The period $[t_0 + t_b, t_0 + t_b + t_r]$ is then considered wet. When time reaches $[t_0 + t_b + t_r]$, the process is repeated to determine the next storm-interstorm sequence. The method assumes rectangular pulses with a uniform rainfall intensity throughout the period t_r.

In regard to temperature, the SWG assumes that the hourly air temperature $T(t)(^\circ C)$ is a sum of two variables: a deterministic air temperature component $T(t)$ and a random variable $\delta T(t)$

$$T(t) = \tilde{T}(t) + \delta T(t) \qquad (8)$$

The deterministic component is built on an empirical method of Bryan (1994) that attributes temporal variation of air temperature to the divergence of radiative heat flux and eddy heat flux. The hourly temperature increments can be regressed on several hydrometeorological variables as

$$\frac{d\widetilde{T}(t)}{dt} = b_0 - b_1 \widetilde{T}(t) + b_2 K(t)s(t) + b_3 K(t)r(t) + b_4 q(t) \qquad (9)$$

where $b_i (i=0,1,\dots,4)$=regression coefficients; $s(t)$ and $r(t)$ =variables of the sun position and geographic location; $K(t)=1 -0.65N^2(t)$=radiation attenuation factor due to cloud cover; and $q(t)$=estimate of incoming longwave radiation. The first-order differential equation can be solved if the initial temperature is provided.

The required parameters for precipitation are the mean value of the time between storms μ_b, the mean storm duration μ_r, and the mean storm depth μ_d. For climates with pronounced seasonality, these parameters should take into account the intraannual variability (Ivanov et al. 2007). The SWG has been calibrated and tested by Ivanov et al. (2007) using long-term data (30 to 35 years) from three weather stations: Albuquerque International Airport (New Mexico), Tucson International Airport (Arizona), and Tulsa International Airport (Oklahoma); the results are consistent with historical observations. The reader is referred to Ivanov et al. (2007) for additional details on the construction, testing and capabilities of the hourly SWG.

Distributed Hydrologic Model

To evaluate water resources availability under current conditions and climate scenarios, the TIN-based real-time integrated basin simulator (tRIBS) has been applied. tRIBS is a physically based, distributed hydrologic model that emphasizes the dynamic relationship between a partially saturated vadose zone and the land surface response to the continuous storm and interstorm cycle. tRIBS explicitly considers the spatial variability in precipitation fields and land-surface descriptors and is capable of resolving basin hydrology at very fine temporal (hourly) and spatial (10–100 m) scales. The model represents the topography of a river basin using a TIN. The irregular spatial discretization given by a TIN allows one to preserve critical hydrologic features in the terrain to properly account for the conceptual understanding of basin dynamics, using just the 5–10% of the original grid nodes (Vivoni et al. 2004,2005). Hydrologic processes are computed using the Voronoi polygons associated with each TIN node. These irregular polygons surround each node and form the basis of the finite-volume computations in the model.

In each polygon, tRIBS simulates the principal land phase hydrologic processes, such as rainfall interception, evapotranspiration, infiltration with continuous soil moisture accounting, lateral moisture transfer in the unsaturated and saturated zones, and overland and channel runoff routing. The model simulates continuously the main component of water and energy balances (see Ivanov et al. 2004a; Vivoni et al. 2007; Noto et al. 2008): rainfall interception based on a canopy water balance model (Rutter et al. 1971); short-wave and long-wave radiation (Bras 1990); surface latent, sensible and ground heat fluxes, computed using the combination equation (Penman 1948; Monteith 1965), gradient method (Entekhabi 2000), and force restore (Hu and Islam 1995). Gravity-dominated infiltration is simulated in a sloped, heterogeneous, and anisotropic soil. The evolution of the wetting and top fronts may lead to unsaturated, perched, surface, and completely saturated states. The unsaturated and saturated zones are thus coupled accounting for the interaction of the moving infiltration front with a variable groundwater surface. A quasi-three-dimensional "cascade" groundwater model allows for lateral water redistribution in the saturated zone and the dynamic interaction with the unsaturated zone. The model estimates surface runoff taking into account four different mechanisms of generation. Infiltration and saturation excess runoff represent the rapid surface response of the basin to rainfall, while perched return flow and groundwater exfiltration represent the slow subsurface response (Vivoni et al. 2007).

In the model, the initial wetness of the basin is controlled by the groundwater position. The spatial distribution of the water table depth represents the primary variable to initialize the model. The initialization methodology for the model is described in detail by Ivanov et al. (2004a) and Vivoni et al. (2005, 2007). The importance of an appropriate initialization for the correct modeling of the basin response has been discussed in detail in Noto et al. (2008), which considered the impact of initial conditions for different combinations of soil type, topography, and precipitation.

Case Study

Study Basins

The aim of this study is the analysis of the effects of climate scenarios at the watershed scale in the Southern Great Plains, in particular for the Baron Fork at Eldon, located in the northeastern corner of Oklahoma, and its subbasin Peacheater Creek at Christie. Fig. 1 shows the location of the basins. Baron Fork at Eldon has an area of $\sim$800 km^2, while the Peacheater Creek is $\sim$65 km^2 in size and are characterized by a mixed land use of forest (52.2%), croplands and orchards (46.3%), and small rural towns (1.3%). The Baron Fork basin has a high stream gauge density and a long historical time series of precipitation radar data (Vivoni et al. 2006). The mean annual discharge for the Baron Fork is $\sim$0.75 m^3/s (mean annual surface runoff of $\sim$360 mm), while the mean annual precipitation over the area is about 1,100 mm (Ivanov et al. 2004b), distributed primarily in the wet fall and spring seasons. Additional details on the climate, hydrology, and basin characteristics have been presented in Vivoni et al. (2005, 2006, 2007) and Ivanov et al. (2004a,b).

Climate Data and Trend Analysis

With the aim of a more accurate quantification of trends in precipitation and temperature for the study area, a trend analysis was carried out to provide a reliable basis for generation of climate scenarios. Monthly, seasonal and annual precipitation and temperature records were obtained from the U.S. Historical Climatology Network (Williams et al. 2007) for the period 1948–2000 from 46 stations in a large area surrounding the Baron Fork basin. Precipitation and temperature series were analyzed using the Mann-Kendall nonparametric test. Trends of precipitation and temperature at the 90, 95, and 99% level of confidence were considered. In order to generate consistent future climate scenarios, the magnitude of significant trends was estimated using Hirsch et al. (1982). The trend analysis has been carried out at local and regional scale, as previously described.

Setup of the Numerical Experiments

Numerical simulations in the Baron Fork and Peacheater Creek were carried out using the tRIBS model with TIN domains of 66,657 and 66,680 nodes, respectively, derived using the procedure described in Vivoni et al. (2004). tRIBS simulations were conducted for scenarios with no trends reflecting the current climate conditions, and with climate scenarios generated based on
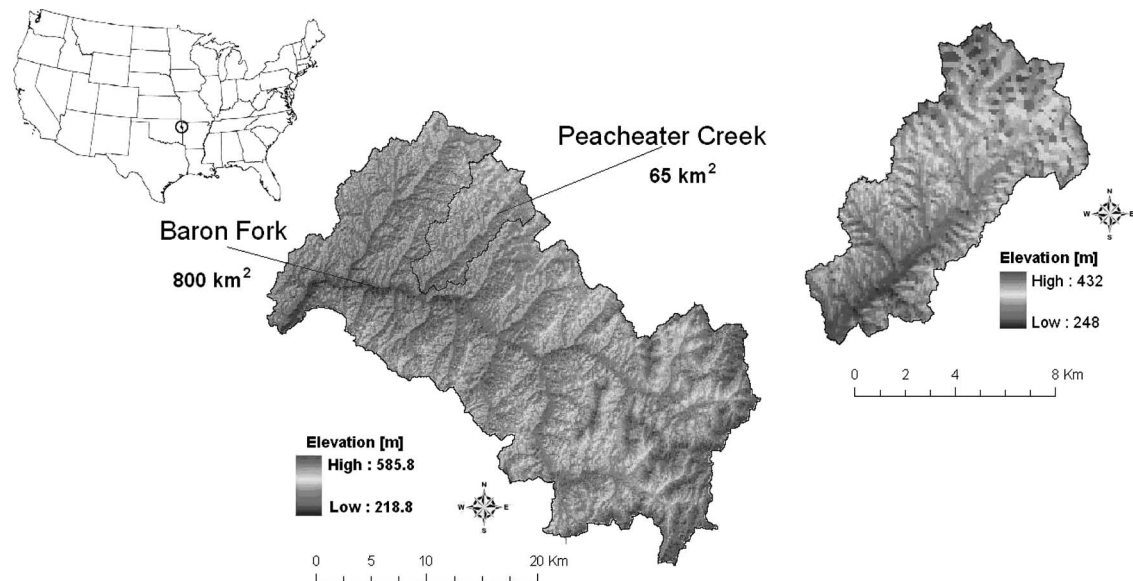
Fig. 1. Location of the study basins and topographic distributions

the trend analysis and SWG. Distributed hydrologic variables were simulated for a 10-year period, assumed long enough to detect the effects of variations of precipitation and temperature on the basin water balance. In each simulation, the hydrometeorological forcings from the SWG were considered uniform across the basin due to the point nature of the method (Ivanov et al. 2007).

Two separate sets of simulations were carried out. In a first group, each scenario consisted of the same initial condition of the basin, i.e., the same spatial distribution of the groundwater table depth at the initial time step. Given the model structure, this implies the same initial conditions in terms of mean soil moisture in the vadose zone for each scenario. Following Vivoni et al. (2007), a spatially variable initial water table distribution with mean depth of ~5 m was set, with the bedrock depth located at 10 m. This value was obtained carrying out a preliminary simulation in which the basin was drained from a saturated state in absence of rain and evapotranspiration until the observed initial baseflow in the basin (Q_b=0.1 m^3/s) was reached. The model initialization procedure is fully described in Ivanov et al. (2004a) and Vivoni et al. (2005, 2007).

A second initialization strategy has been considered since a climate trend could imply that future scenarios can have different initial conditions. For each scenario, this is taken into account by using the initialization strategy of Vivoni et al. (2005) consisting of the creation of a spin-up period, characterized by periodic forcing. In this study, the spin-up is a three years period that repeats a one-year set of hydrometeorological variables which are different for each scenario. In this way, the final conditions of the basin from the three-year period will be different for each case in terms of the spatial distribution of groundwater table depth (mean depth varies from 3.4 to 4.5 m). These final conditions are then used as initial conditions in the 10-year simulations.

Results and Discussion

Trend Analysis Results and Generation of Climate Scenarios

The trend analysis in precipitation at the annual, seasonal and monthly scales was carried out using the nonparametric Mann-

Kendall test. A general positive trend of the annual precipitation was detected at a confidence level of 90% (Table 1). At the seasonal scale, the trend analysis was performed for four periods: winter (January–March), spring (April–June), summer (July–September) and fall (October–December). Results shown in Table 1 indicate that positive precipitation trends are predominant in winter and fall at the rate of ~6% and ~4% per decade, respectively, while only a few positive trends have been detected in spring. At the monthly scale, a significant positive trend was observed only in three months, November, December and March at the rate of 3%, 9%, and 10% per decade, respectively (Table 1). These results are in good agreement with the analysis by Garbrecht et al. (2004) in which the writers detected an annual and seasonal increase of precipitation over the period 1981–2001. These writers also found that late springs, early summer and fall

Table 1. Precipitation Trend Analysis

Precipitation time scale	Confidence interval			Magnitude [mm/year]
	90%	95%	99%	
Annual	•/+	○	○	4
Winter	•/+	•/+	○	1
Spring	○	○	○	—
Summer	○	○	○	—
Fall	•/+	•/+	○	1
January	○	○	○	—
February	○	○	○	—
March	•/+	○	○	0.4
April	○	○	○	—
May	○	○	○	—
June	○	○	○	—
July	○	○	○	—
August	○	○	○	—
September	○	○	○	—
October	○	○	○	—
November	•/+	•/+	○	0.8
December	•/+	○	○	0.5

Note: The black dot indicates trend existence; the "+" sign indicates positive trend; the white dot indicates absence of significant trend.

Table 2. Precipitation Trend Analysis and Magnitudes in Seven Seasonal Periods

Precipitation seasonal period	Confidence interval			Magnitude [mm/year]
	90%	95%	99%	
December–February	•/+	•/+	∘	2
March–April	•/+	•/+	∘	1
May	∘	∘	∘	—
June	∘	∘	∘	—
July–August	∘	∘	∘	—
September	∘	∘	∘	—
October–November	•/+	•/+	∘	1.5

months had a larger portion of the annual precipitation increase. According to Garbrecht et al. (2004), the average precipitation increase (statistically significant) over the watershed was about 14% over the period 1981–2001, while according to the trend analysis the rate of increase over 20 years is ~9%.

As discussed previously, the SWG has been tested at three meteorological stations (Ivanov et al. 2007). For our case study, meteorological data for Tulsa International Airport in the vicinity of the basins have been obtained from Automatic Surface Observing System and used to generate the climate forcing for each scenario. For the Tulsa precipitation data, seven periods were identified by Ivanov et al. (2007) for seasonal predictions: December–February, March–April, May, June, July–August, September, and October–November. As a result, SWG parameters need to account for intraannual variability. For this reason, an additional set of trend analyses were performed for each season. Results in Table 2 indicate a positive trend with a 90% level of confidence in the precipitation seasons: December–February, March–April and October–November. In addition, Table 2 reports the magnitude of significant trends detected in the seven precipitation seasons. The period December–February is characterized by a 1.8% rate of increase per year, while in the March–April and October–November, the increases are at the 0.5% and 0.8% per year, respectively.

With regard to temperature, the Mann-Kendall test indicated the absence of a significant trend in annual, seasonal and monthly temperatures over the study period. In particular, the mean annual temperature shows the presence of a significant positive trend in only 5% of the 46 stations, at a confidence level of 90%. At the seasonal scale, a small number of positive temperature trends were identified in winter, while spring and fall temperatures show weak decreases limited to a small percentage of stations. In most cases, the percentage of sites with a temperature trend is too low to assert that a regional trend is occurring. Moreover, the Mann-

Kendall regional test and the bootstrap technique detected the absence of statistically significant trend in the basin, as corroborated by the IPCC (2007). As a result, it is possible to conclude that the study region does not show a general temperature trend and we do not pursue this effect in the numerical simulations.

Results obtained from the trend analysis were used to make consistent hypothesis in the generation of climate scenarios. The expected climate changes (i.e., positive trend in precipitation, no trend in temperature) are imposed on the observed values of the climate parameters used in the SWG. In a climate projection, the detected positive trends of precipitation at a seasonal scale can be reproduced in the model by an increase of the mean storm depth (μ_d) or an increase of the mean storm duration (μ_r) or by a combination of these. For these reasons, the mean storm depth and storm duration have been modified separately according to the detected trend for the precipitation seasons that show statistically significant trends, i.e., December–February, March–April, and October–November.

Since the climate system of the Earth is strongly nonlinear, its development can be forecast only to a limited degree (Lorenz 1963). For these reasons, assumptions are needed in climate scenario generation. Here, the assumption of a climate system in "equilibrium" has been used (i.e., with stationary mean values of climatic parameters), by comparing different scenarios with different stationary mean values. This is one of the possible approaches used in a majority of impact studies of climate change on agricultural yields and sea-level rise (e.g., Carter et al. 1992). An alternative approach (Favis-Mortlock and Boardman 1995) is to model the nonequilibrium ("transient") situation, where the statistical properties of climatic variables are not assumed stationary.

Using the equilibrium approach, two groups of scenarios have been created: Group A increases the mean storm depth, while Group B increases the mean storm duration. Each group has three scenarios: climate projection to years 2020, 2050, and 2100. Each scenario is denoted with an alphanumeric string in which the first letter denotes the group and the number indicates the climate projection year. The hydrometeorological variables of the no-trend scenario have been generated using the SWG, with parameters obtained from historical data at Tulsa (see Table 3).

In this study, climate scenarios have been generated supposing that changes in precipitation, detected by the trend analysis, will proceed in the future with the same pattern, assuming the hypothesis of a linear trend. With regard to the Group A scenarios, starting from the seasonal trend analysis, the rate of increase in precipitation has been identified in each season that shows a trend. This rate, calculated as a ratio between the magnitude of the trend and the mean precipitation in the season, was then multiplied for the number of years in each scenario, starting from the

Table 3. Parameters of the SWG for Tulsa Precipitation Data for the No-Trend Scenario, and for Scenarios of Groups A and B

| Scenario	Parameter	December–February	March–April	May	June	July–August	September	October–November
No-trend	μ_r [mm]	0.98	1.95	3.04	3.41	3.01	2.61	1.91
	μ_d [h]	6.82	5.46	4.06	3.86	3.91	4.86	6.66
	μ_b [h]	107.37	75.15	60.03	69.47	102.16	73.08	104.14
A2020	μ_r [mm]	1.18	2.15	3.04	3.41	3.01	2.61	2.29
A2050		1.47	2.54	3.04	3.41	3.01	2.61	2.86
A2100		1.96	3.13	3.04	3.41	3.01	2.61	3.82
B2020	μ_d [h]	8.18	6.00	4.06	3.86	3.91	4.86	8.00
B2050		10.23	7.09	4.06	3.86	3.91	2.61	10.00
B2100		13.64	8.73	4.06	3.86	3.91	2.61	13.33
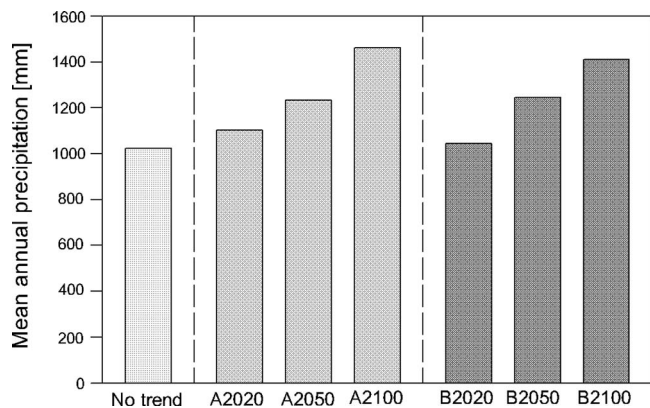
Fig. 2. Mean annual precipitation (mm) in each scenario

year 2005 (i.e., the parameters of the scenario A2020 are obtained multiplying the rate of increase for 15 years). Group B scenarios were created by making the hypothesis that the increase in precipitation could be due to an increase of the mean storm duration. The rate of this increase is the same used to generate the Group A scenarios. In this case, the ratio was multiplied for the number of years as well. Table 3 summarizes of the values of mean storm depths and mean storm durations.

For each scenario, the hydrometeorological variables have been stochastically generated for a period of 10 years, considered long enough to detect effects of precipitation variations on the basin water balance. Precipitation is the only input variable that changes in the simulations as shown in Fig. 2. The mean annual precipitation for the no-trend scenario is 1,024 mm/year, consistent with the observations at the site. Comparing the mean annual precipitation of the no-trend scenario with Group A scenarios, the increase is about 8%, 20%, and 42%, respectively. For Group B scenarios, the mean annual precipitation increases by 2%, 21%, and 38% for the B2020, B2050, and B2100, respectively. The mean seasonal precipitation of each scenario of Groups A and B are shown in Fig. 3, indicating that the spring and winter are characterized by higher values.

Overview of Hydrologic Model Results and Water Resources Analysis

Surface runoff and the main components of the water balance have been estimated using tRIBS for the no-trend scenario and for the six scenarios to assess impacts of precipitation trends on surface and groundwater resources. The impact on surface water resources was evaluated using the percentage of the increase of surface runoff with respect to the increase of precipitation. Moreover, the exceedance curves for streamflow were analyzed in each scenario. Subsequently, the variations of the groundwater volume were assessed to determine groundwater resources. We present results for Peacheater Creek basin using the two different initialization strategies of the model. Once the influence of initialization is discussed, results for Baron Fork basin are described. In the analysis, both lumped and distributed metrics of the hydrologic sensitivity to the climate change scenarios are present. The distributed representations include spatial distributions of the basin response.

Peacheater Creek Basin

Effects of Precipitation Trends on Water Balance and Surface Water Resources

The annual water balance, calculated as $\Delta S/\Delta t = P - ET - R$, provides information on the effects of precipitation (P) changes on the watershed response, including the total storage (S), evapotranspiration (ET), and runoff (R). Table 4 shows the mean annual values for the water balance components for the no trend and Groups A and B scenarios, for both initialization strategies. The results indicate that the increasing precipitation trend has a strong impact on surface runoff and a comparatively weaker effect on ET, probably due to the absence of a temperature trend. Hydrologic simulations with different initializations lead to greater ET and R, with comparably smaller storage changes ($\Delta S/\Delta t$), for the same precipitation input as the scenarios with constant initial conditions.

Table 5 shows that a percentage change in precipitation (PCP, %) produces a larger percentage change in runoff (PCR, %) and a smaller percentage change in ET (PCET, %). Analysis of the sensitivities of runoff to precipitation (SR) and the sensitivities of evapotranspiration to the precipitation (SET) variations confirms these results (Table 5). Sensitivities were estimated as the ratio of the relative increase in ET and R over the relative increase of precipitation (SR=PCR/PCP and SET=PCET/PCP). In addition, the initialization condition appears to have minor effects on the sensitivities (SET and SR), except for the ratio SR of scenario B2020, which equal to 5.5. This similarity underlines that wetter initial conditions does not produce a marked effect on the percent-
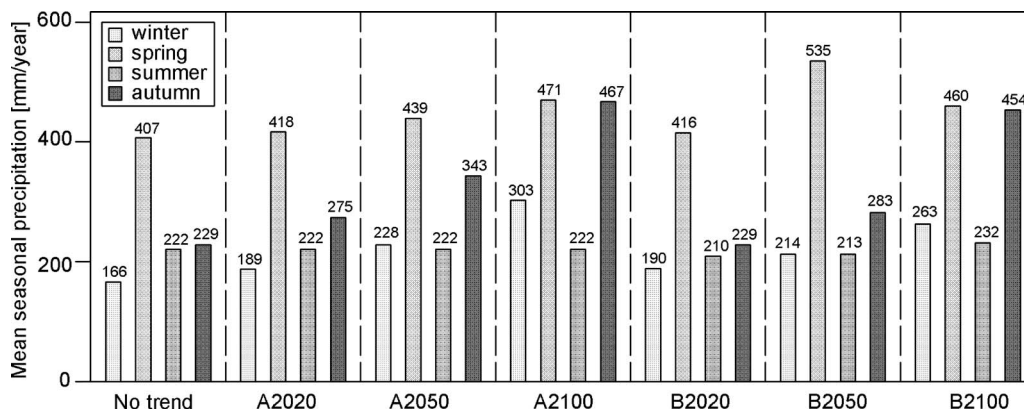

Fig. 3. Mean seasonal precipitation (mm) in each scenario of Groups A and B

Table 4. Water Balance Components for the Climate Scenarios in Groups A and B under Identical and Different Initialization Strategies

Scenario		P [mm/year]	ET [mm/year]	R [mm/year]	$\Delta S / \Delta t$ [mm/year]
No-trend		1,024.0	753.56	234.73	35.70
Same initialization	A2020	1,103.2	768.97	292.63	41.59
	A2050	1,232.5	787.06	395.65	49.78
	A2100	1,462.7	808.06	592.83	61.81
	B2020	1,044.4	756.61	249.43	38.35
	B2050	1,245.1	794.83	393.24	57.03
	B2100	1,409.7	805.30	539.60	64.79
Different initialization	A2020	1,103.2	773.95	312.02	17.23
	A2050	1,232.5	792.13	420.99	19.38
	A2100	1,462.7	812.49	625.58	24.63
	B2020	1,044.4	762.01	277.66	4.73
	B2050	1,245.1	801.22	442.30	1.58
	B2100	1,409.7	809.49	577.40	22.81

age increase of runoff and evapotranspiration with respect to the no-trend condition. However, the presence of a rising groundwater table results in a small increase of mean annual runoff and evapotranspiration. For simulations of Groups A and B for each initialization, the range of variations of increases of runoff varies from 6 to 24% for the projections to 2020, from 57 to 76% for the projections to 2050, and from 129 to 152% for the projections to 2100. With regard to evapotranspiration, the range of variations of increases is 0.4–2.1% (2020), 4.5–5.7% (2050), and 6.8–7.2% (2100). Clearly, in each climate scenario the ranges of variation of runoff are wider than for evapotranspiration.

In the study by Garbrecht et al. (2004), the sensitivities of runoff and evapotranspiration to variations of precipitation were measured in a similar fashion. According to the writers, the runoff-precipitation sensitivity for Baron Fork is ~3.3, in agreement with our simulations which range from 3.1 to 3.6. Nevertheless, the evapotranspiration-precipitation sensitivity in Garbrecht et al. (2004) is close to zero, while the simulations exhibit sensitivities ranging from 0.2 to 0.3. This discrepancy is likely due to the simplifying assumption by the writers in the calculation of evapotranspiration as a residual, ET=$P-R$. This assumption effectively ignores the changes in basin storage at the annual scale, which are not negligible, as shown in Table 4. As a result, this sensitivity analysis is in agreement for R and provides a slight improvement for ET, as compared to Garbrecht et al. (2004).

Differences among the climate scenarios are further highlighted through the mean monthly streamflow shown in Fig. 4 for the different initialization conditions. Mean monthly streamflows increase from the no-trend scenario to the A2100 and B2100 scenarios. In both groups of scenarios, the monthly mean streamflow peaks in the spring (March to May) and fall (November), and has a minimum in summer (August to September). Scenarios of Group A are characterized by similar temporal patterns, with minimal differences in peak flow timing, up to 2 months for the spring and negligible differences in the fall. In scenarios A2020, A2050 and A2100, a marked increase of streamflow in spring is observed, while minor increases occur in summer months. In contrast, scenarios of Group B exhibit large differences in the temporal pattern of mean monthly streamflow, as the variations of the mean storm duration produce changes in peak runoff. In addition, Group B scenarios show significant variations in peak magnitude and streamflow seasonality, which are not progressive from the B2020 to the B2100 cases. Monthly mean streamflow for the

Table 5. Changes in Precipitation, Runoff, and Evapotranspiration for Scenarios of Groups A and B, in Millimeters per Year [mm/year] and Percentage (%) Relative to the No-Trend Simulation

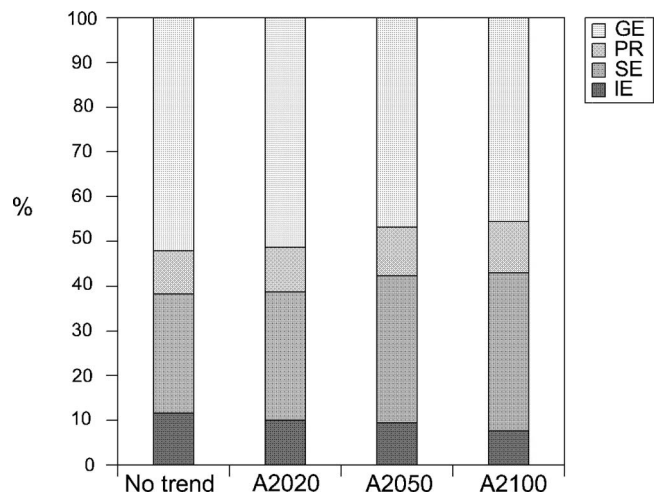| Scenario		P Δ [mm/year]	(%)	R Δ [mm/year]	(%)	ET Δ [mm/year]	(%)	SR	SET
Same initialization	A2020	79.2	7.7	57.9	24.7	15.4	2.0	3.2	0.3
	A2050	208.5	20.4	160.9	68.6	33.5	4.4	3.4	0.2
	A2100	438.7	42.8	358.1	152.5	54.5	7.2	3.6	0.2
	B2020	20.4	2.0	14.7	6.3	3.1	0.4	3.1	0.2
	B2050	221.1	21.6	158.5	67.5	41.3	5.5	3.1	0.3
	B2100	385.7	37.7	304.9	129.9	51.7	6.9	3.4	0.2
Different initialization	A2020	79.2	7.7	62.1	24.8	16.0	2.1	3.2	0.3
	A2050	208.5	20.4	171.0	68.4	34.2	4.5	3.4	0.2
	A2100	438.7	42.8	375.6	150.3	54.6	7.2	3.5	0.2
	B2020	20.4	2.0	27.7	11.1	4.1	0.5	5.5	0.3
	B2050	221.1	21.6	192.3	76.9	43.3	5.7	3.6	0.3
	B2100	385.7	37.7	327.4	131.0	51.6	6.8	3.5	0.2

Note: SR=sensitivity of runoff to variation in precipitation and SET=sensitivity of evapotranspiration to variation in precipitation.
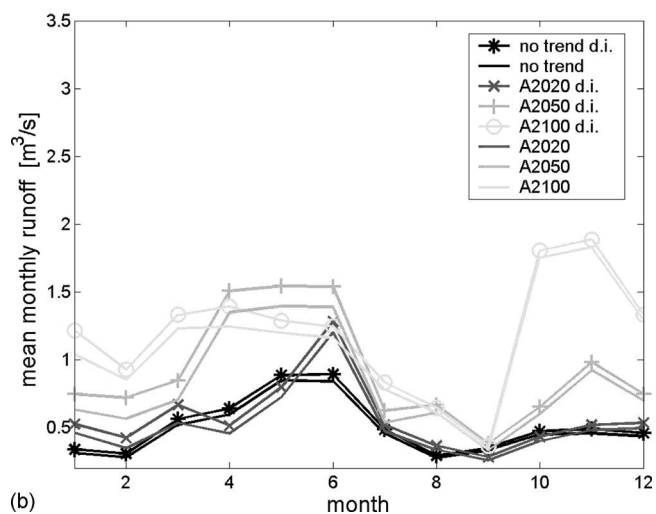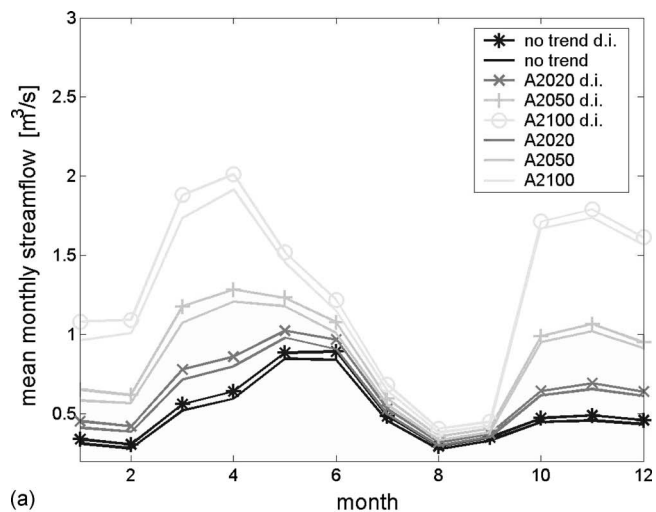
Fig. 4. Mean monthly runoff (mm) for: (a) Group A; (b) Group B scenarios

Fig. 5. Runoff partitioning in the Group A scenarios for the same initial water table positions: groundwater exfiltration (GE), perched return (PR), saturation excess (SE), and infiltration excess (IE) runoff components

simulations characterized by different initial water table depth (labeled with d.i. in Fig. 4) are similar to the constant initialization cases, exhibiting 5–10% more streamflow during each month.

In regards to seasonal streamflow, Table 6 shows the percentage variation of streamflow in each scenario compared with the no-trend case. By comparing the mean seasonal streamflow in each scenario, winter and autumn are the seasons characterized by high increases. With regard to winter, the increases range from 20 to 233%; for spring the streamflow percentage variations are

between 4 and 98%; summer shows the lower increases, ranging from 0.2 to 62%; while the range of variation for autumn streamflow varies from 2.6 to 270%.

Precipitation trends also affect the runoff partitioning, as shown in Fig. 5 for the Group A scenarios (similar results for Group B, not shown). Precipitation increases, either due to higher mean storm depth or duration, lead to a higher runoff percentage by the saturation excess runoff and perched return mechanisms, while infiltration excess runoff and groundwater exfiltration decrease. However, the distribution of surface runoff (infiltration excess and saturation excess runoff) and subsurface runoff (perched return flow and groundwater exfiltration) does not show pronounced changes. Substantially, the runoff decrease due to infiltration excess is compensated by the increase in runoff from saturation excess. Similar compensation occurs between perched return flow and groundwater exfiltration. Therefore, the presence of a trend in precipitation does not produce a considerable effect on the runoff partitioning of runoff. Similar results (not shown) were obtained when considering the simulations with different initial positions of the groundwater table.

The effect of precipitation increases on surface water resources was evaluated through exceedance curves, which show the number of days during which the mean daily discharge is exceeded at the basin outlet (Fig. 6). The two scenario groups are characterized by a progressive increase of the available surface water resources. To assess the surface water volumes available, a hypo-

Table 6. Variation (%) of Mean Seasonal Streamflow in Each Scenario of Groups A and B Compared with the No-Trend Case

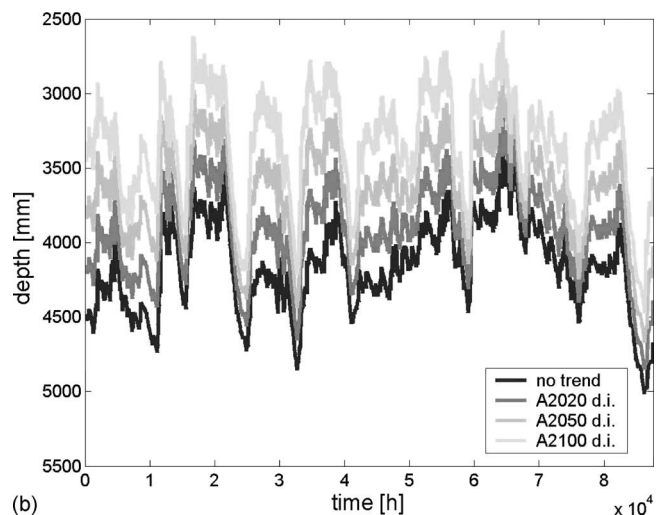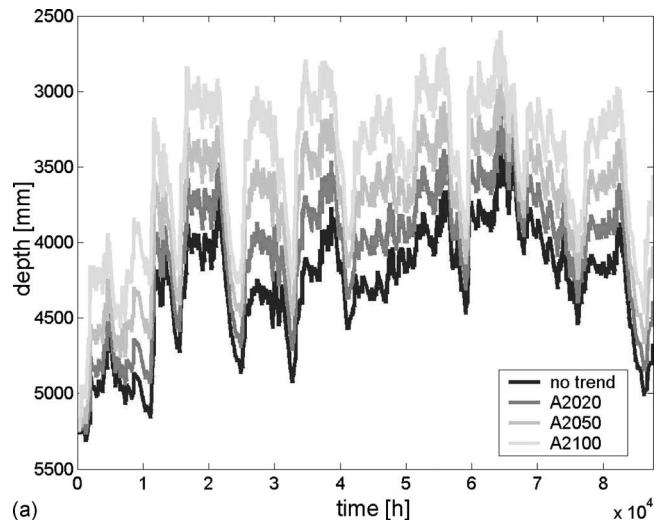| Scenario	Seasonal mean streamflow							
	Winter	(%)	Spring	(%)	Summer	(%)	Autumn	(%)
No-trend	0.37	—	0.76	—	0.35	—	0.45	—
A2020	0.50	35.9	0.90	17.7	0.38	8.0	0.63	40.5
A2050	0.74	99.9	1.13	48.8	0.42	19.8	0.96	115.2
A2100	1.24	233.3	1.51	98.1	0.48	36.4	1.66	271.1
B2020	0.45	20.7	0.79	4.4	0.35	0.2	0.46	2.6
B2050	0.63	70.7	1.38	81.2	0.49	39.3	0.74	65.5
B2100	1.04	180.6	1.20	57.9	0.58	62.7	1.62	263.4
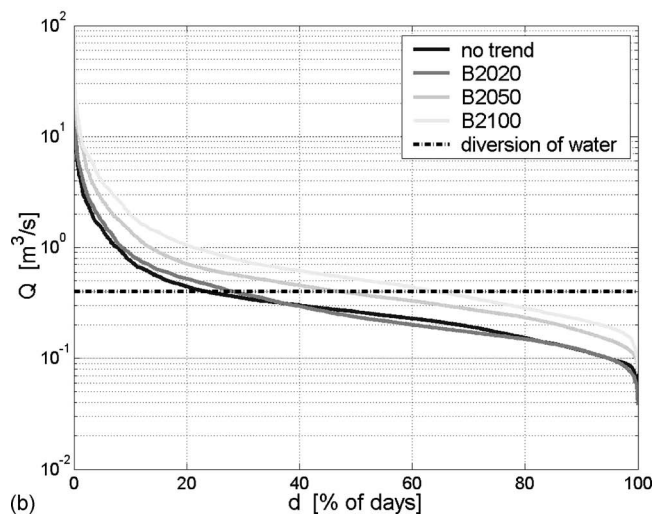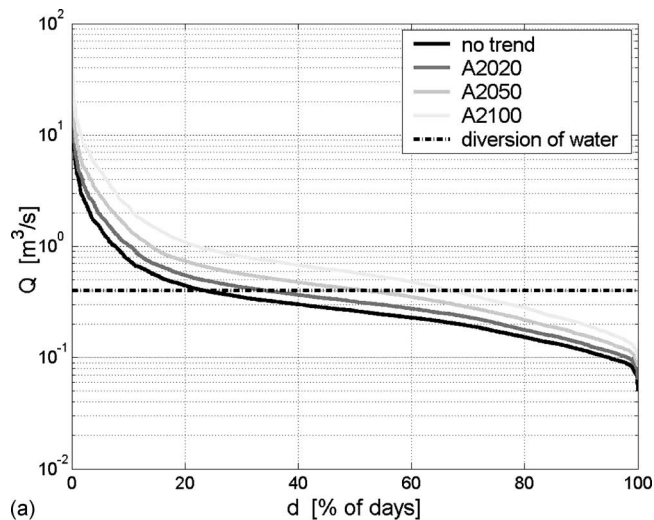
Fig. 6. Exceedance curves for the climate scenarios in: (a) Group A; (b) Group B for the same initial groundwater table positions
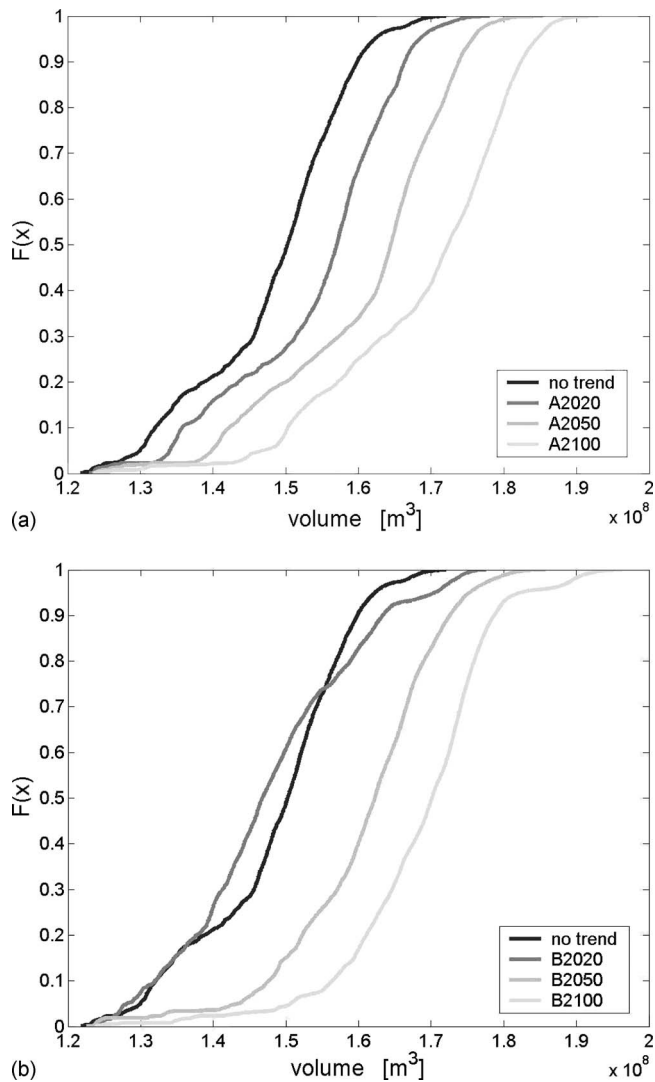

Fig. 7. Mean groundwater table depth time series for Group A scenarios under: (a) same initial groundwater table positions; (b) different initial groundwater table positions

thetical extraction at the basin outlet with a maximum divertible amount equal to 0.4 m^3/s (smaller than the mean daily discharge of the no-trend case, 0.8 m^3/s) is used. In Fig. 6, the water diversion is represented with the exceedance curves as a horizontal line. The area under each exceedance curve and the diversion line represents the volume available for the water supply. This volume clearly increases from the no trend to the A2100 and B2100 scenarios. Table 7 summarizes the volume of water that can be di-

Table 7. Available Volumes of Water for Diversion in Each Scenario of Groups A and B

Scenario	Volume [Mm³]
No-trend	83.62
A2020	93.23
A2050	103.24
A2100	111.00
B2020	83.76
B2050	102.86
B2100	111.69

verted in 10 years, considering the 0.4 m^3/s threshold. Similar results (not shown) were obtained for the simulations with different initial water table depth.

Effects of Precipitation Trends on Groundwater Resources
The initialization strategy needs to be considered when assessing the impact of precipitation trends on the simulated groundwater resources. To illustrate this, Fig. 7 presents the time series of the mean depth to the water table for the no trend and Group A scenarios (changes in mean storm depth) for the constant and different initial conditions. The increase in mean annual precipitation from scenarios A2020 to A2100 progressively produces a rising of the water table toward the land surface. For the constant initialization, all scenarios exhibit the same water table at the beginning of the simulation [Fig. 7(a)]. For the different initializations, the periodic forcing during the spin-up leads to conditions that better reflect the long-term impact of precipitation trends on the initial state [Fig. 7(b)]. Nevertheless, the impact of the initial conditions is quickly dissipated within the first 3 years of the 10-year simulations, such that the effects at the final state are expected to be minimal.

Fig. 8. CDF of groundwater volumes for: (a) Group A; (b) Group B scenarios under the same initial groundwater table positions

Differences in available groundwater resources were estimated by comparing the CDF of groundwater volumes for the constant initialization (Fig. 8). Groundwater volumes were computed as the spatially distributed difference between the water table and bedrock depths times the aquifer porosity. Positive precipitation trends clearly results in a larger amounts of groundwater resources. Table 8 compares the mean groundwater volumes, illustrating a 4%, 9%, and 14% increase for the A2020, A2050, and A2100 scenarios, respectively. For the Group B scenarios, changes of 0.4%, 8%, and 14% were recorded in the B2020, B2050, and B2100 case relative to the no-trend scenario, respectively. For simulations of Groups A and B for each initialization, the range of variations of increases of volumes varies from 2.3 to 4.5% for the projections to 2020, from 5.9 to 9.6% for the projections to 2050, and from 13.2 to 15% for the projections to 2100. These small percentages point out the slight positive effect of the precipitation trend on groundwater resources. Similar results are obtained for the simulations with the different initial conditions. This indicates that a positive precipitation trend, occurring either as an increase of mean storm depth or duration, produces similar increases on groundwater resources for long simulations.

Table 8. Mean Annual Groundwater Volumes for Scenarios in Groups A and B; the Percentages Refer to the Changes with respect to the No-Trend Scenario

Scenario		Volume [Mm^3]			
		Mean	(%)	Median	(%)
Same initialization	A2020	154.30	4.0	157.01	4.5
	A2050	161.14	8.6	164.44	9.5
	A2100	168.98	13.9	172.31	14.7
	B2020	147.71	0.4	146.76	−2.3
	B2050	160.67	8.3	162.23	8.0
	B2100	168.49	13.6	170.10	13.2
Different initialization	A2020	147.71	4.2	146.76	4.3
	A2050	160.67	5.9	162.23	6.9
	A2100	168.49	14.0	170.10	15.0
	B2020	152.22	0.4	151.67	−0.1
	B2050	166.29	9.6	166.30	9.6
	B2100	172.33	13.6	173.04	14.0

By comparing the variation of surface and groundwater resources, it can be concluded that the increase of groundwater due to precipitation trend is less marked than the increase of surface water resources. Table 9 summarizes the variation of surface and groundwater resources. The ratio of the variation of surface water resources to the variation of groundwater resources (SRV/GRV) has been calculated in each scenario. Results show that the increase of surface water resources is ~3 times greater than the increase of groundwater resources in the scenarios of Group A and B.

Peak over Threshold (POT) Analysis

Positive precipitation trends produce an increase in both surface and groundwater resources, which may have beneficial regional impacts in terms of water supply. These positive effects, however, could be tempered by negative impacts, including an increasing flood risk. To quantify the flood frequency in the Peacheater Creek, a peak over threshold (POT) analysis was conducted. The characteristics of the method are described in Madsen et al. (1997) and Lang et al. (1999). The POT approach involves two main steps: selection of a flood threshold and estimation of the number of events exceeding the threshold. Three streamflow (Q) thresholds were selected (30, 50, and 100 m^3/s) for the analysis based on the historical observations in the basin. Table 10 presents the number of events exceeding the three thresholds for each scenario. Precipitation increases imply a growing of number of peaks over the threshold, in particular for the Group A (mean storm depth) scenarios. Comparison of Groups A and B indicates that increases in mean storm depth are more important in inducing flood events as compared to increases in storm duration. The

Table 9. Surface and Groundwater Resources Variation (%) and Their Ratio in Each Scenario

Scenario	SRV (%)	GRV (%)	SRV/GRV (-)
A2020	11.5	4	2.9
A2050	23.5	8.6	2.7
A2100	32.7	13.9	2.4
B2020	0.2	0.4	0.4
B2050	23.0	8.3	2.8
B2100	33.6	13.6	2.5

Table 10. Number of Events Exceeding the Streamflow (Q) Thresholds for Each Scenario of Groups A and B

Scenario		$Q > 30$ [m³/s]	$Q > 50$ [m³/s]	$Q > 100$ [m³/s]
No-trend		38	24	4
Same initialization	A2020	51	24	4
	A2050	90	37	4
	A2100	220	67	4
	B2020	42	8	0
	B2050	88	10	0
	B2100	169	40	11
Different initialization	A2020	52	25	4
	A2050	92	37	4
	A2100	227	71	4
	B2020	47	12	0
	B2050	103	12	0
	B2100	194	53	13

number of events is greater in the cases of long-term climate projections (A2100 and B2100), in particular for the lower flood threshold ($Q > 30$ m³/s). In the case of threshold $Q > 30$ m³/s, for simulations of Groups A and B for each initialization, the range of variations of increases of the number of POT varies from 42 to 52 for the projections to 2020, from 88 to 103 for the projections to 2050, and from 170 to 227 for the projections to 2100. However, a reduction in the number of POT was obtained for Group B scenarios for the largest thresholds ($Q > 50$ or 100 m³/s), except during the B2100 cases, which exhibit a large increase. This implies that major flood events induced by a trend in the mean storm duration do not linearly increase with the positive precipitation trend.

Baron Fork Basin

As indicated previously, simulations in the Peacheater Creek basin were conducted using the two different strategies of initializations. Since these simulations indicated only a slight influence of the initialization technique, simulations for Baron Fork have been performed using the same initial conditions in each scenario. In the following sections, an abbreviated description of the Baron Fork results will be presented, including an analysis of the simulated soil moisture patterns.

Effects of Precipitation Trends on Water Balance and Surface Water Resources

Similar hydrometeorological forcings were used to create hydrological model simulations over the Baron Fork for the scenarios in Groups A and B. A positive precipitation trend produced an increase of streamflow, consistent with simulations at Peacheater Creek. The mean annual runoff for Baron Fork of 107.58 mm is underestimated in the no-trend scenario as compared to historical observations ($\sim$350 mm). On the other hand, the mean annual evapotranspiration of 977.05 mm is higher than the simulations in the subbasin Peacheater Creek and the calculated value by Garbrecht et al. (2004) of $\sim$760 mm. These water balance differences for Baron Fork suggest that the assumption of spatially uniform precipitation forcing made here may not be adequate at this basin scale ($\sim$800 km²). Previous simulations by Ivanov et al. (2004b) with precipitation radar data matched the annual basin water balance much better. For the smaller Peacheater Creek ($\sim$65 km²), use of the SWG at the point scale is more appropriate.

While biases in the water balance components are important, the sensitivity analysis to the precipitation trends were carried out to reveal the differences at the scale of the Baron Fork. Table 11 presents the sensitivity analysis of runoff and evapotranspiration changes relative to precipitation trends. Clearly, a percentage change in precipitation produces a larger PCR (%) and a smaller PCET (%). The relative increase in runoff with respect to precipitation (SR) ranges from 2.8 to 9.2, which is greater than the sensitivity found for Peacheater Creek and values reported in Garbrecht et al. (2004). This suggests that the precipitation trends at the larger scale of the Baron Fork yield greater impacts on streamflow in the future scenarios as compared to the historical data. The evapotranspiration-precipitation sensitivity (SET), on the other hand, ranges from 0.2 to 0.3, consistent with results in Peacheater Creek basin. This indicates that the overestimation of the mean annual ET in the Baron Fork does not impact its sensitivity to precipitation changes.

The effect of precipitation increases on the surface water resources was evaluated through the analysis of the exceedance curves. Under the assumption of a maximum divertible amount of 1.5 m³/s, the no-trend case yields a mean annual volume of water divertible at the outlet of $\sim$38.76 Mm³. This volume increases by 10%, 20%, and 30% for the A2020, A2050, and A2100 scenarios, respectively, while the water availability for the Group B scenarios exhibit slightly lower increases: 1%, 20%, and 25%, respectively, for the B2020, B2050, and B2100 scenarios.

Table 11. Changes in Precipitation, Runoff, and Evapotranspiration for Scenarios of Groups A and B, in Millimeters per Year [mm/year] and Percentage (%) Relative to the No-Trend Simulation in Baron Fork

	P		R		ET			
Scenario	Δ [mm]	(%)	Δ [mm]	(%)	Δ [mm]	(%)	SR	SET
A2020	79.20	7.7	39.9	37.1	26.95	2.8	4.8	0.4
A2050	208.50	20.4	123.6	114.9	59.95	6.1	5.6	0.3
A2100	438.70	42.8	305.4	283.9	96.65	9.9	6.6	0.2
B2020	20.40	2.0	19.7	18.3	3.78	0.4	9.2	0.2
B2050	221.10	21.6	116.2	108.0	70.65	7.2	5.0	0.3
B2100	385.70	37.7	255.6	237.6	85.45	8.7	6.3	0.2

Note: SR=sensitivity of runoff to variation in precipitation and SET=sensitivity of evapotranspiration to variation in precipitation.
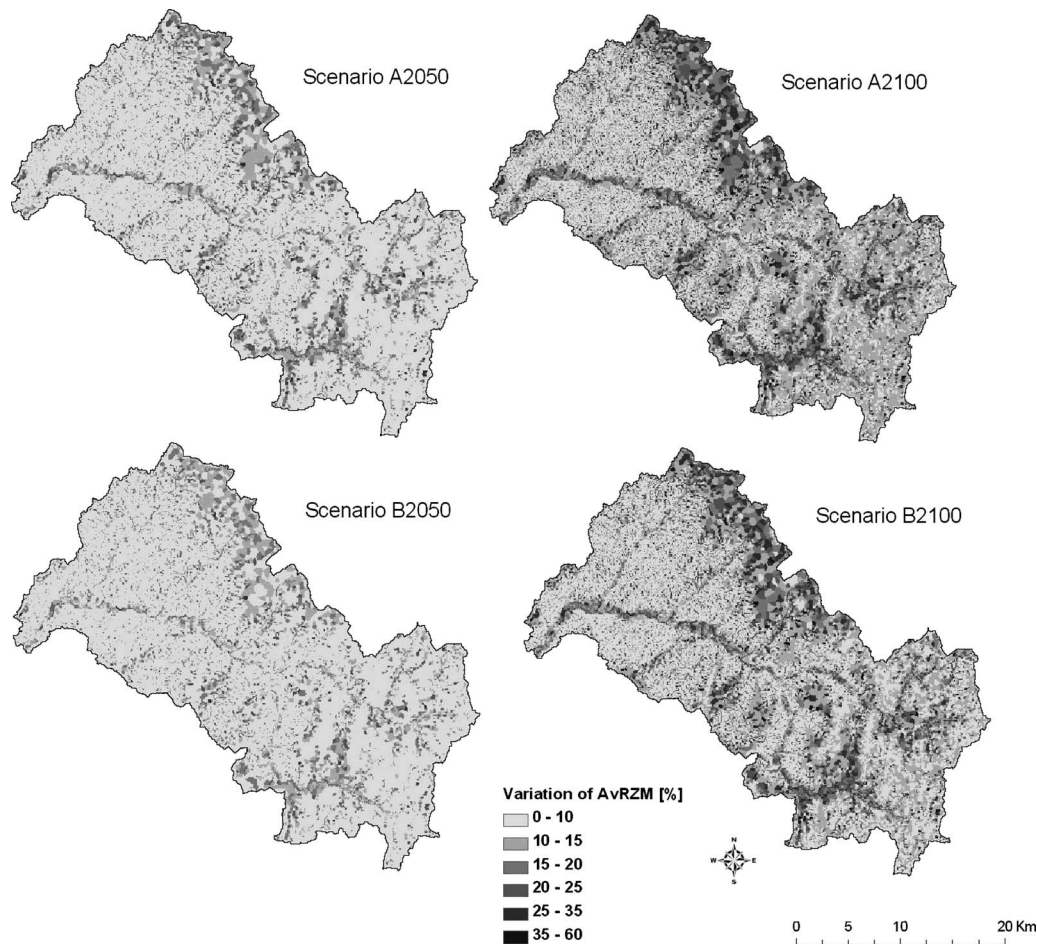
Fig. 9. Spatial distribution of the percentage variation of the time-averaged soil moisture in the root zone (AvRZM) of scenarios A2050, A2100, B2050, and B2100 as compared to the no-trend scenario

Effects of Precipitation Trends on Groundwater Resources

Comparing the mean groundwater volumes, Group A and B scenarios shows similar results for the Baron Fork. In particular, an increase of the mean groundwater volumes in the simulations A2020 and B2020 presents a slight increase (0.5%) compared to the no-trend case. For the A2050 and B2050 scenarios, the percentage increase of stored volume is about 20% and 11%, respectively, while the A2100 and B2100 have 32% and 31% increases. These results are higher than the ones obtained for the subbasin Peacheater Creek, except the scenarios A2020 and B2020, that are characterized by a slight increase of groundwater volumes for both basins.

Example of Spatial Variability of Hydrological Response

The use of a distributed model also allows assessing the spatial variability of the hydrologic response. The tRIBS simulations under the climate change scenarios provide dynamic spatial maps of the water table depth, evapotranspiration, and soil moisture in the root zone (top 1 m), among others. Fig. 9 shows the spatial distribution of the change of time-averaged root zone soil moisture in the A2100 and B2100 scenarios as compared to the no-trend case. Spatial distributions are similar, suggesting that the increase of precipitation, due to either an increase of storm depths or durations, produces the same effect on the soil moisture pattern. The most significant root zone soil moisture increases are located along the river network and in the northern flat areas of the basin, that are characterized by a higher frequency of satura-

tion excess runoff, due to the gradual rising of the water table. These spatially distributed results are useful for assessing potential climate change impacts on the local water and energy balance for agricultural or environmental purposes.

Conclusions

In this study, the effects of climate change on water resources availability of an operational-scale basin in northeastern Oklahoma was investigated using the tRIBS model. The distributed hydrologic model was used to estimate the basin water balance components and the surface and groundwater availability for current conditions and a set of climate scenarios. Numerical simulations were carried out for the Peacheater Creek and Baron Fork basins, considering a no-trend scenarios and scenarios created based on a trend analysis of precipitation and temperature observations for the study region. The multitemporal trend analysis revealed an increase in precipitation for particular seasons and the absence of a statistically significant change in temperature. To capture the precipitation trends, two groups of scenarios were created using an increase in the mean storm depth and the mean storm duration parameters.

The analysis of the results obtained by the application of tRIBS to the test basins provided some important conclusions about the implications of climate change in the Southern Great

Plains region. With regard to the two test basins, results can be summarized as follows:

1. The distributed hydrologic model translates the changes of precipitation in each scenario to the basin runoff and evapotranspiration response. The increase in precipitation produces an increase of available surface and groundwater resources. The increase of surface water resources is ~3 times greater than the increase of groundwater resources in each scenario of Group A and B. Evapotranspiration seems to only be slightly affected by the trend due to higher soil moisture in the basin induced by the greater precipitation and the absence of a temperature trend.

2. Sensitivity analyses of the evapotranspiration and runoff changes to precipitation variations confirm these results and are in good agreement with the analysis carried out by Garbrecht et al. (2004). However, the sensitivity of evapotranspiration to the variation of precipitation in Garbrecht et al. (2004) is close to zero, while in the scenarios of this study they range from 0.2 to 0.3. This discrepancy is probably due to the simplifying assumption by the writers in the calculation of evapotranspiration as a residual of the difference between precipitation and runoff. However, it is important to remark that the results provided here are due to an imposed precipitation trend, while results of Garbrecht et al. (2004) are referred to variations of precipitation over a certain period.

3. The analysis of exceedance curves for each climate scenario showed that the trend of precipitation implies an increase of exploitable surface water resources of 12, 24, and 33% for A2020, A2050, and A2100, respectively, and similar percentage for scenarios of Group B, except for B2020, in which the positive trend of storm durations has a small impact (0.2% more) on surface water volumes. On the other hand, this trend also increases the flood risk in the basin, as determined using the POT analysis. In addition, comparison of the CDF of groundwater volumes showed an increase of available groundwater resources.

4. A set of simulations were carried out considering different initial conditions of the basin (Peacheater Creek) since the presence of a precipitation trend could imply that in future scenarios the basin would be characterized by wetter initial conditions. Results showed that results are slightly affected by the initialization of the model, in particular the use of wetter initial condition for the basin implies a small increase of surface runoff, and does not affect evapotranspiration.

5. Simulations in the larger Baron Fork basin showed similar results, i.e., the mean annual runoff is more sensitive to changes in precipitation than the mean annual evapotranspiration. This behavior is probably due to the absence of a significant trend of temperature for the study region. However, the mean annual runoff obtained for the no-trend case is lower than the value obtained from historical data. This underestimation is probably due to the assumption of uniform forcings over the basin.

These findings are of interest in water resources planning and management, as an indicator of the potential changes that could affect water resources availability in the study area. In future work, an analysis of water demand in the area (in particular for agricultural activities) may provide insight on the apportioning of the water resources available from the climate change impacts. This study also reveals that distributed hydrologic models provide the detailed sensitivity of water balance components to hydrometeorological trends resulting from climate change.

Nevertheless, some final remarks need to be made about climate change impacts studies. This study follows a commonly used sequence of models or analytical procedures to relate climate change to a water resources impact: first, a trend analysis is carried out; second, a stochastic method is used to generate synthetic variables of a climate scenario; finally, a hydrological model is calibrated and tested using observed streamflow and meteorological data, and then forced with climate change scenarios. Each step of this sequence is associated with a degree of uncertainty, which affects the direction and magnitude of the estimated impacts. It is important to remark that a climate scenario is not intended to explicitly represent real future climate, since it represents one of all possible climate realizations. Scenarios used in climate change impacts studies commonly focus on mean climate change, while few studies have considered detailed, explicit changes in variability (Wilks 1992; Mearns and Rosenzweig 1997; Barrow and Semenov 1995). Moreover, in climate change scenario generation, the assumption of a climate system in equilibrium is frequently used (i.e., with stationary mean values), while the climate system is strongly nonlinear. In conclusion, the assessment of climate change implications on water resources is highly dependent on the scenarios considered and the models used to simulate the hydrological processes. The reliability of the estimated impacts of climate change on surface and groundwater hydrology is affected by large uncertainties. Nevertheless, these studies provide useful information about the quantification of the potential effects of climate change, in order to develop new strategies to deal with these changes.

Acknowledgments

References

Arnell, N. W. (1999). "Climate change and global water resources." *Global Environ. Change*, 9, S31–S49.

Barrow, E., and Semenov, M. A. (1995). "Climate change scenarios with high spatial and temporal resolution for agricultural applications." *J. Forest.*, 68, 349–360.

Bras, R. L. (1990). *Hydrology: An introduction to hydrologic science*, Addison-Wesley, Reading, Mass.

Bryan, J. G. (1994). *Short range hour-by-hour forecast of temperature by projecting the characteristic curve with constants fitted to immediately preceding data*, Travelers Res. Cent., Inc., Hartford, Conn.

Carter, T. R., Parry, M. L., Nishioka, S., and Harasawa, H. (1992). *Preliminary guidelines for assessing impacts of climate change*, Environmental Change Unit/Center for Global Environmental Research, Oxford, U.K.

Christensen, N. S., Wood, A. W., Voisin, N., Lettenmaier, D. P., and Palmer, R. N. (2004). "Effects of climate change on the hydrology and water resources of the Colorado River Basin." *Clim. Change*, 62, 337–363.

Degelman, L. O. (1991). "A statistically-based hourly weather data generator for driving energy simulation and equipment design software for buildings." *Proc., Building Simulation '91 Conf.*, Nice, France, 592–599.

Douglas, E. M., Vogel, R. M., and Kroll, C. N. (2000). "Trends in floods in the United States: Impact of spatial correlation." *J. Hydrol.*, 240, 90–105.

Duell, L. F. W. (1994). "The sensitivity of northern Sierra Nevada streamflow to climate change." *Water Resour. Bull.*, 30(5), 841–859.

Easterling, D. R., Meehl, G. A., Parmesan, C., Changnon, S. A., Karl, T. R., and Mearns, L. O. (2000). "Climate extremes: Observations, modeling, and impacts." *Science*, 289, 2068–2074.

Efron, B. (1979). "Bootstrap methods: Another look at the jack knife." *Ann. Stat.*, 7, 1–26.

Entekhabi, D. (2000). *Land surface processes: Basic tools and concepts*, Dept. of Civil and Environmental Engineering, MIT, Cambridge, Mass.

Favis-Mortlock, D., and Boardman, J. (1995). "Nonlinear responses of soil erosion to climate change: A modelling study on the UK South Downs." *Catena*, 25, 365–387.

Garbrecht, J., and Rossel, F. E. (2002). "Decade-scale precipitation increase in Great Plains at end of 20th century." *J. Hydrol. Eng.*, 7(1), 64–75.

Garbrecht, J., Rossel, F. E., and Schneider, J. M. (2001). "Decade-scale precipitation and streamflow variation in the Kansas-Nebraska region." *Proc., 12th Symp. on Global Change and Climate Variations*, 81st American Meteorological Society Annual Meeting, Americal Meterological Society, Albuquerque, N.M., 319–321.

Garbrecht, J., Van Liew, M., and Brown, G. O. (2004). "Trends in precipitation, streamflow, and evapotranspiration in the great plains of the United States." *J. Hydrol. Eng.*, 9(5), 360–367.

Grotch, S., and MacCracken, M. (1991). "The use of general circulation models to predict regional climate change." *J. Clim.*, 4, 286–303.

Hamlet, A. F., and Lettenmaier, D. P. (1999). "Effects of climate change on hydrology and water resources in the Columbia River basin." *J. Am. Water Resour. Assoc.*, 35, 1597–1623.

Hirsch, R. M., Slack, J. R., and Smith, R. A. (1982). "Techniques of trend analysis for monthly water quality data." *Water Resour. Res.*, 18, 107–121.

Hu, Q., Woodruff, C. M., and Mudrick, S. E. (1998). "Interdecadal variations of annual precipitation in the central United States." *Bull. Am. Meteorol. Soc.*, 79(2), 221–229.

Hu, Z., and Islam, S. (1995). "Prediction of ground surface temperature and soil moisture content by the force-restore method." *Water Resour. Res.*, 31, 2531–2539.

IPCC. (1995). *The science of climate change*, J. T. Houghton, L. G. Meira Filho, B. A. Callander, N. Harris, A. Kattenberg, and K. Maskell, eds., Cambridge University Press, Cambridge, U.K.

IPCC. (2007). *The physical science basis working group I contribution to the fourth assessment report of the IPCC*, S. Solomon, D. Qin, M. Manning, M. Marquis, K. Averyt, M. M. B. Tignor, and H. L. Miller, eds., Cambridge University Press, Cambridge, U.K.

Ivanov, V. Y., Bras, R. L., and Curtis, D. C. (2007). "A weather generator for hydrologic, ecological, and agricultural applications." *Water Resour. Res.*, 43, W10406.

Ivanov, V. Y., Vivoni, E. R., Bras, R. L., and Entekhabi, D. (2004a). "Catchment hydrologic response with a fully-distributed triangulated irregular network model." *Water Resour. Res.*, 40, W11102.

Ivanov, V. Y., Vivoni, E. R., Bras, R. L., and Entekhabi, D. (2004b). "Preserving high-resolution surface and rainfall data in operational-scale basin hydrology: A fully-distributed physically-based approach." *J. Hydrol.*, 298(1–4), 80–111.

Karl, T. R., and Knight, R. W. (1998). "Secular trends of precipitation amount, frequency and intensity in the United States." *Bull. Am. Meteorol. Soc.*, 79, 231–241.

Karl, T. R., Knight, R. W., Easterling, D. R., and Quayles, R. G. (1996). "Indices of climate change for the United States." *Bull. Am. Meteorol. Soc.*, 77, 279–292.

Kendall, M. G. (1962). *Rank correlation methods*, 3rd Ed., Hafner, New York.

Kunkel, K. E., Andsager, K., and Easterling, D. R. (1999). "Long-term trends in extreme precipitation events over the conterminous United States and Canada." *J. Clim.*, 12, 2515–2527.

Lang, M., Ouarda, T. B. M. J., and Bobee, B. (1999). "Towards operational guidelines for over-threshold modeling." *J. Hydrol.*, 225, 103–117.

Leavesley, G. H. (1994). "Modeling the effects of climate change on water resources—A review." *Clim. Change*, 28, 159–177.

Lettenmaier, D. P., Wood, A. W., Palmer, R. N., Wood, E. F., and Stakhiv, E. Z. (1999). "Water resources implications of global warming: A U.S. regional perspective." *Clim. Change*, 43, 537–579.

Lettenmaier, D. P., Wood, E. F., and Wallis, J. R. (1994). "Hydroclimatological trends in the continental United States." *J. Climatol.*, 7, 586–607.

Lorenz, E. N. (1963). "Deterministic nonperiodic flow." *J. Atmos. Sci.*, 20, 130–141.

Madsen, H., Rasmussen, P. F., and Rosjbierg, D. (1997). "Comparison of annual maximum series and partial duration series methods for modeling extreme hydrologic events. 1: At site modeling." *Water Resour. Res.*, 33(4), 747–757.

Mann, H. B. (1945). "Non-parametric tests against trend." *Econometrica*, 13, 245–259.

McCarthy, J. J., Canziani, O. F., Leary, N. A., Dokken, D. J., and White, K. S. (2001). "Climate change 2001: Impacts, adaptation and vulnerability." *Contribution of working group II to the third assessment report of the intergovernmental panel on climate change*, Cambridge University Press, Cambridge, U.K.

Mearns, L. O., and Rosenzweig, C. (1997). "Formation of climate change scenarios incorporating changes in daily climate variability and application to crop models." *Assessing climate change: The story of the model evaluation consortium for climate assessment*, W. Howe and A. Henderson-Sellers, eds., Chapter 15, Harwood Academic.

Mearns, L. O., Rosenzweig, C., and Goldberg, R. (1997). "Mean and variance change in climate scenarios: Methods, agricultural applications, and measures of uncertainty." *Clim. Change*, 35(4), 367–396.

Monteith, J. L. (1965). "Evaporation and environment." *Symp. Soc. Exp. Biol.*, 19, 205–234.

Nash, L. L., and Gleick, P. H. (1991). "Sensitivity of streamflow in the Colorado Basin to climatic changes." *J. Hydrol.*, 125, 221–241.

Nash, L. L., and Gleick, P. H. (1993). "The Colorado River Basin and climatic change: The sensitivity of streamflow and water supply to variations in temperature and precipitation." *Rep. No. EPA230-R-93-009*, EPA, Washington, D.C.

Nemec, J., and Schaake, J. (1982). "Sensitivity of water resource systems to climate variation." *J. Hydrol. Sci.*, 27, 327–343.

Noto, L. V., Ivanov, V. Y., Bras, R. L., and Vivoni, E. R. (2008). "Effects of initialization on response of a fully-distributed hydrologic model." *J. Hydrol.*, 352, 107–125.

Parlange, M. B., and Katz, R. W. (2000). "An extended version of the Richardson model for simulating daily weather variables." *J. Appl. Meteorol.*, 39, 610–622.

Penman, H. L. (1948). "Natural evaporation from open water, bare soil and grass." *Proc. R. Soc. London, Ser. A*, 193, 120–145.

Richardson, C. W. (1981). "Stochastic simulation of daily precipitation, temperature, and solar radiation." *Water Resour. Res.*, 17, 182–190.

Rutter, A. J., Kershaw, K. A., Robins, P. C., and Marton, A. J. (1971). "A predictive model of rainfall interception in forests. I: Derivation of the model from observations in a plantation of Corsican Pine." *Agric. Meterol.*, 9, 367–384.

Semenov, M. A., and Barrow, E. M. (1997). "Use of a stochastic weather generator in the development of climate change scenarios." *Clim. Change*, 35, 397–414.

Smith, M. B., et al. (2004). "The distributed model intercomparison project (DMIP): Motivation and experiment design." *J. Hydrol.*, 298(1–4), 4–26.

Vivoni, E. R., et al. (2006). "Extending the predictability of hydrometeorological flood events using radar rainfall nowcasting." *J. Hydrometeor.*, 7(4), 660–677.

Vivoni, E. R., Entekhabi, D., Bras, R. L., and Ivanov, V. Y. (2007). "Controls on runoff generation and scale-dependence in a distributed hydrologic model." *Hydrology Earth Syst. Sci.*, 11(5), 1683–1701.

Vivoni, E. R., Ivanov, V. Y., Bras, R. L., and Entekhabi, D. (2004).

"Generation of triangulated irregular networks based on hydrologic similarity." *J. Hydrol. Eng.*, 9(4), 288–302.

Vivoni, E. R., Ivanov, V. Y., Bras, R. L., and Entekhabi, D. (2005). "On the effects of triangulated terrain resolution on distributed hydrologic model response." *Hydrolog. Process.*, 19, 2101–2122.

Werner, P. C., and Gerstengarbe, F.-W. (1997). "A proposal for the development of climate scenarios." *Clim. Res.*, 8, 171–182.

Wilby, R. L., Hay, L. E., and Leavesley, G. H. (1999). "A comparison of downscaled and raw GCM output: Implications for climate change scenarios in the San Juan River basin, Colorado." *J. Hydrol.*, 225, 67–91.

Wilks, D. S. (1992). "Adapting stochastic weather algorithms for climate change studies." *Clim. Change*, 22, 67–84.

Wilks, D. S., and Wilby, R. L. (1999). "The weather generation game: A review of stochastic weather models." *Prog. Phys. Geogr.*, 23, 32–357.

Williams, C. N., Jr., Menne, M. J., Vose, R. S., and Easterling, D. R. (2007). "United States historical climatology network monthly temperature and precipitation data." *Rep. No. ORNL/CDIAC-118, NDP-019*, Carbon Dioxide Information Analysis Center, Oak Ridge National Laboratory, U.S. Dept. of Energy, Oak Ridge, Tenn., ⟨http://cdiac.ornl.gov/epubs/ndp/ushcn/usa_monthly.html⟩ (October 2008).

Wolock, D. M., and McCabe, G. J. (1999). "Estimates of runoff using water-balance and atmospheric general circulation models." *J. Am. Water Resour. Assoc.*, 35, 1341–1350.

Wood, A. W., Leung, L. R., Sridhar, V., and Lettenmaier, D. P. (2004). "Downscaling climate model surface precipitation and temperature: A comparison of methods." *Clim. Change*, 62, 189–216.

Yates, D., Gangopadhyay, S., Rajagopalan, B., and Strzepek, K. (2003). "A technique for generating regional climate scenarios using a nearest neighbor algorithm." *Water Resour. Res.*, 39(7), 1199.